Inorganic Chemistry

ARTICLE

pubs.acs.org/IC

Structural Variability in Ag(I) and Cu(I) Coordination Polymers with Thioether-Functionalized Bis(pyrazolyl)methane Ligands

Irene Bassanetti and Luciano Marchiò*

Dipartimento di Chimica Generale ed Inorganica, Chimica Analitica, Chimica Fisica, Università degli Studi di Parma, parco Area delle Scienze 17/a, I 43124 Parma, Italy

Supporting Information

ABSTRACT: We present here two ligand classes based on a bis(pyrazolyl)methane scaffold functionalized with a rigid (-Ph-S-Ph) or flexible (-CH_2-S-Ph) thioether function: L^RPhS (R = H, Me) and $L^R CH_2S$ (R = H, Me, iPr). The X-ray molecular structures of Ag(I) and Cu(I) binary complexes with L^RPhS or $L^R CH_2S$ using different types of counterions (BF_4^-, PF_6^-, and $CF_3SO_3^-$) are reported. In these complexes, the ligands are N_2 bound on a metal center and bridge on a second metal with the thioether group. In contrast, when using triphenylphosphine (PPh_3) as an ancillary ligand, mononuclear ternary complexes $[M(L)PPh_3]^+$ (M = Cu(I), Ag(I); L = L^RPhS, $L^R CH_2S$) are formed. In these complexes, the more flexible ligand type, $L^R CH_2S$, is able to provide the N_2S chelation, whereas the more rigid L^RPhS ligand class is capable of chelating only N_2 because the thioether function preorganized, as it did in the coordination polymers, to point away from the metal center. Rigid potential-energy surface scans were performed by means of density functional theory (DFT) calculations (B3LYP/6-31+G) on the two representative ligands, L^HPhS and $L^H CH_2S$. The surface scans proved that the thioether function is preferably oriented on the opposite side of the bispyrazole N_2 chelate system. These results confirm that both ligand classes are suitable components for the construction of coordination polymers. Nevertheless, the methylene group that acts as a spacer in $L^H CH_2S$ imparts an inherent flexibility to this ligand class so that the conformation responsible for the N_2S chelation is energetically accessible.

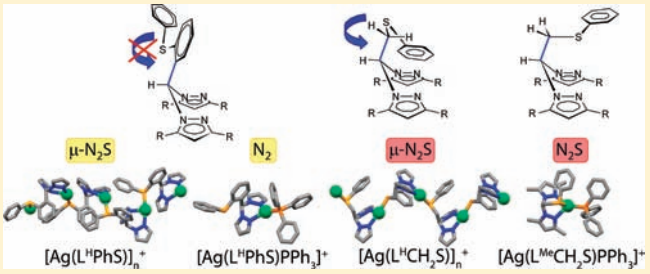

INTRODUCTION

The rational design of coordination polymers has produced a wide variety of interesting solid-state structures that are useful in the development of new functional materials.[1−4] The possible applications of these various 1- to 3-dimensional systems can be grouped into diverse fields such as catalysis,[5] gas adsorption[6] (gas separation[7] and gas storage[8,9]), molecular recognition,[10] luminescence,[11,12] magnetism,[13,14] and drug delivery.[15] The ability to design multitopic organic ligands that can bind the metal center in a predictable way, as determined by their preferred conformation, is crucial to the development of coordination architectures. In this respect, the ligands may be defined as rigid or flexible according to the high or low energy barrier, respectively, that separates two or more ligand conformers.[16] Specific ligands can also be designed to be configurationally rigid, and they can impart peculiar electronic properties upon binding to a metal.[17] The choice of the metal atom as the node in the construction of coordination polymers is also important because its stereoelectronic requirements, that is, coordination numbers and geometry, heavily influence the overall shape of the resulting polymer. Ag(I) is a fashionable metal node for the construction of coordination polymers, and it has been used extensively for this purpose. The lack of a crystal-field effect allows for the occurrence of different coordination geometries, but the most common are the linear, trigonal-planar, T-shaped, and tetrahedral geometries. Many examples of Ag(I) coordination polymers in which the nature of the donor ligand may lead to the formation of different frameworks with tailored structures and functions have been reported in the literature.[18−26] In addition to classical metal−donor coordination bonds, silver is apt to give rise to metallophilic (Ag−Ag)[27] and σ or π organometallic (Ag−C) interactions with aromatic moieties.[28−32]

Multitopic bis(pyrazolyl)methane ligands are currently being studied for the design of coordination polymers, and the choice of the spacer between two or three bis-pyrazolyl donor functions influences the structure of the resulting molecular architectures.[33−38] The spacer can be either rigid, as in aromatic groups,[35] or more flexible, as in alkylidene chains,[36] and the different conformational degrees of freedom have important consequences on the coordination properties of these ligands. In fact, the aromatic spacer group, when compared to alkylidene chains, allows better control over the formation of polymeric structures.[35] The group attached to a bis(pyrazolyl)methane scaffold can also be functionalized with carboxylate moieties, and the formation of silver polymeric structures has been achieved by the direct interaction of this group with the metal atom or by the formation of bridging hydrogen bonds.[39]

Received: June 22, 2011
Published: October 03, 2011

Scheme 1. Ligand Synthesis

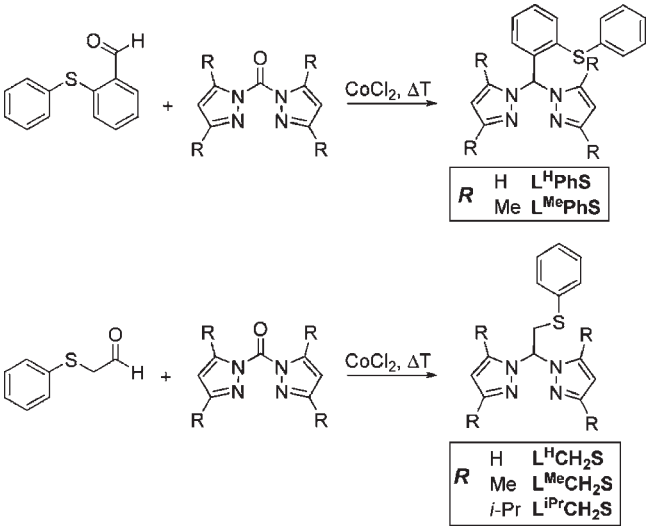

In our previous work, we used a ditopic N_2S_2 heteroscorpionate ligands based on a bis(pyrazolyl)methane system that was functionalized with a bis-thioether function to prepare Ag(I) complexes. The spacer between the N_2 and S_2 donor systems was rigid (Ph group), and this resulted in the opposite orientation of the N_2 and S_2 chelate system so that coordination polymers were preferentially formed with Ag(I). The steric hindrance of the pyrazole rings also exhibited a considerable influence on the donor ability of the ligand, because the presence of iPr groups hindered the metal coordination of one of the thioether moieties.[40]

In the present work, we wish to present two ligand classes based on the bis(pyrazolyl)methane system functionalized with a rigid (-Ph-S-Ph) and flexible (-CH_2-S-Ph) thioether function: L^RPhS (R = H, Me) and L^RCH_2S (R = H, Me, iPr) (Scheme 1). The molecular structures of Ag(I) and Cu(I) complexes with L^RPhS or L^RCH_2S using different types of counterions (BF_4^-, PF_6^-, and $CF_3SO_3^-$) are reported, and they show how the flexibility or rigidity of the thioether group influences the formation of polymeric structures. Ternary complexes using triphenylphosphine (PPh_3) as an ancillary ligand of the type $[M(L^RPhS)PPh_3]$ and $[M(L^RCH_2S)PPh_3]$ (M = Cu(I) and Ag(I)) are also described, and they more clearly show the different conformational behaviors of the two ligand classes. In addition, density functional theory (DFT) calculations are employed to investigate the energetics pertaining to the mobility of the pyrazole rings and the two thioether groups in L^HPhS and L^HCH_2S. These calculations show that, in L^HPhS, the thioether function is preferably oriented toward the $CH_{central}$ and is therefore on the opposite side of the N_2 system (rigid ligand). At variance, L^HCH_2S is characterized by a greater inherent flexibility that allows for N_2S chelation and the bridging behavior between two metal centers.

EXPERIMENTAL SECTION

1,1′-((2-(Phenylthio)phenyl)methylene)bis(1*H*-pyrazole) (L^HPhS), 1′-((2-(phenylthio)phenyl)methylene)bis(3,5-dimethyl-1*H*-pyrazole) ($L^{Me}PhS$), 1,1′-(2-(phenylthio)ethane-1,1-diyl)bis(1*H*-pyrazole) (L^HCH_2S), 1′-(2-(phenylthio)ethane-1,1-diyl)bis(3,5-dimethyl-1*H*-pyrazole) ($L^{Me}CH_2S$), and 1′-(2-(phenylthio)ethane-1,1-diyl)bis(3,5-diisopropyl-1*H*-pyrazole) ($L^{iPr}CH_2S$) were synthesized as previously described.[41−44] The syntheses of these ligands were performed under inert gas (N_2) using Schlenk techniques. The solvents were dried and distilled before use. All other reagents and solvents were commercially available. ^1H NMR spectra were recorded on a Bruker Avance 300 spectrometer using standard Bruker pulse sequences. Chemical shifts are reported in parts per million (ppm) and referenced to residual solvent protons ($CDCl_3$, CD_3CN, $(CD_3)_2CO$, CD_2Cl_2). Infrared spectra were recorded from 4000 to 700 cm^{-1} on a Perkin-Elmer FT-IR Nexus spectrometer equipped with a Thermo-Nicolet microscope. Elemental analyses (C, H, and N) were performed with a Carlo Erba EA 1108 automated analyzer.

The synthesis of binary complexes $[M(L)]^+$ was performed by mixing equimolar amounts of $[Cu(CH_3CN)_4]BF_4$ or Ag(I) salts (anions: BF_4^-, PF_6^-, and $CF_3SO_3^-$) and the appropriate ligand, whereas the $[M(L)(PPh_3)]^+$ ternary complexes were prepared by mixing equimolar amounts of metal salts, ligand, and PPh_3. These syntheses were performed in acetone or in acetonitrile, and the details are provided in the Supporting Information together with the crystallization conditions.

X-ray Crystallography. Single-crystal data were collected on a Bruker Smart 1000 and a Bruker Smart APEXII area-detector diffractometers (Mo Kα; λ = 0.71073 Å). Cell parameters were refined from the observed setting angles and detector positions of selected strong reflections. Intensities were integrated from several series of exposure frames that covered the sphere of reciprocal space.[45] A multiscan absorption correction was applied to the data using the program SADABS.[46] The structures were solved by direct methods (SIR97[47,48] and SIR2004[48]) and refined with full-matrix least-squares (SHELXL-97),[49] using the Wingx software package.[50] Graphical material was prepared with the Mercury 2.0[51] program. CCDC 828865−828884 contain the supplementary crystallographic data for this paper.

DFT Calculations. Rigid potential-energy surface (PES) scans were performed for the L^HCH_2S and L^HPhS ligands starting from the ligand conformations found in the X-ray structures of complexes $[Ag(L^HPhS)]_n(BF_4)_n$ and $[Ag(L^HCH_2S)]_n(BF_4)_n$, respectively. The calculations were performed using the gradient-corrected hybrid density functionals B3LYP[52,53] and the 6-31+G basis set.[54,55] In particular, the PES scan was performed for L^HCH_2S by rotating three molecular fragments: (1) one pyrazole ring (360° rotation about the $C_{central}$-N_{pz} bond: 15 steps, 24°), (2) the CH_2 linker (360° rotation about the $C_{central}$-CH_2 bond: 15 steps, 24°), and (3) the peripheral phenyl ring (180° rotation about the S-Ph bond: 10 steps, 18°). The PES scan for L^HPhS was performed by the following rotations: (1) one pyrazole ring (360° rotation about the $C_{central}$-N_{pz} bond: 15 steps, 24°), (2) the phenyl ring linker (360° rotation about the $C_{central}$-Ph bond: 15 steps, 24°), and (3) the peripheral phenyl ring (180° rotation about the S-Ph bond: 10 steps, 18°). To gain insights on the different binding abilities of the two ligand classes (L^RCH_2S and L^RPhS), we optimized the geometries of two coordination isomers for each model complex, $[Ag(L^HCH_2S)PH_3]^+$ and $[Ag(L^HPhS)PH_3]^+$. The isomers were differentiated by the presence or absence of the thioether coordination to the metal center. The PH_3 ancillary ligand was used instead of the PPh_3 one, which is present in some reported X-ray structures, to save computational resources. The optimizations of the geometries were performed with the B3LYP density functional, with the 6-31+G(d) basis set for C, H, N, S, and P and with the SDD valence basis set and MWB28 effective core potentials for Ag.[56−58] Vibrational frequencies were calculated at the same theoretical level to ensure that the stationary points were true minima. All the calculations were performed with the Gaussian 03 software.[59]

RESULTS AND DISCUSSION

The synthesis of ligands is described in Scheme 1. The synthetic route to obtain C-centered functionalized bis(pyrazolyl)methane ligands is based on solid-state reaction between bis(pyrazolyl)-ketones and aldehydes bearing the desired sulfur donor group

Table 1. Summary of X-ray Crystallographic Data for $[Ag(L^{H}PhS)]_n(BF_4)_n$, $[Cu(L^{H}PhS)(CH_3CN)]_2(BF_4)_2$, and $[Ag(L^{H}PhS)]_2(PF_6)_2 \cdot CH_2Cl_2$

	$[Ag(L^{H}PhS)]_n(BF_4)_n$	$[Cu(L^{H}PhS)(CH_3CN)]_2(BF_4)_2$	$[Ag(L^{H}PhS)]_2(PF_6)_2 \cdot CH_2Cl_2$
empirical formula	$C_{38}H_{32}Ag_2B_2F_8N_8S_2$	$C_{42}H_{38}B_2Cu_2F_8N_{10}S_2$	$C_{40}H_{36}Ag_2Cl_2F_{12}N_8P_2S_2$
formula weight	1054.20	1047.64	1340.37
color, habit	colorless, block	colorless, block	colorless, block
crystal size, mm	0.47 × 0.32 × 0.13	0.20 × 0.12 × 0.05	0.19 × 0.17 × 0.12
crystal system	monoclinic	monoclinic	triclinic
space group	$P2_1/a$	$C2/c$	$P\bar{1}$
a, Å	21.368(1)	26.105(3)	10.160(2)
b, Å	10.170(1)	8.080(1)	10.620(2)
c, Å	21.555(2)	21.356(2)	12.736(2)
α, deg.	90	90	78.688(3)
β, deg.	118.776(1)	99.832(2)	73.156(3)
γ, deg.	90	90	71.562(3)
V, Å^3	4105.7(6)	4438.4(9)	1239.4(4)
Z	4	4	1
T, K	293(2)	190(2)	293(2)
ρ (calc), Mg/m^3	1.705	1.568	1.796
μ, mm^{-1}	1.132	1.131	1.240
θ range, deg.	2.16 to 28.37	1.58 to 27.05	1.68 to 27.10
no.of rflcn/unique	56570/10270	18698/4837	14504/5407
GOF	1.044	1.006	1.004
$R1^a$	0.0554	0.0521	0.0391
$wR2^a$	0.1314	0.0773	0.0813

^{a} $R1 = \Sigma||F_o| - |F_c||/\Sigma|F_o|$, $wR2 = [\Sigma w(F_o^2 - F_c^2)^2/\Sigma w(F_o^2)^2]^{1/2}$, $w = 1/[\sigma^2(F_o^2) + (aP)^2 + bP]$, where $P = [\max(F_o^2,0) + 2F_c^2]/3$.

that were to be attached to the bis(pyrazolyl)methane scaffold. The N_2S donor set of the ligand described in this work is generated by treating substituted bis(pyrazolyl)ketones with (phenylthio)benzaldehyde and (phenylthio)acetaldehyde using $CoCl_2$ hydrate as a catalyst and heating at 110 °C overnight. According to the nature of the thioether arm on the carbon center linking the two pyrazole rings, the ligands can be divided in two classes: the first class exhibits a phenyl group that links the bis(pyrazolyl)methane scaffold to the thioether moiety ($L^{R}PhS$), whereas the second class presents a methylene group as a linker ($L^{R}CH_2S$). Moreover, within each ligand class, the steric hindrance on the pyrazole ring increased when hydrogen atoms at positions 3 and 5 were substituted with methyl or isopropyl groups. We have employed Ag(I) and Cu(I) cations to investigate the different coordinative behaviors of the two ligand classes. The complexes were prepared by treating equimolar amounts of ligands and $[Cu(MeCN)_4]BF_4$ or Ag(I) salts ($AgBF_4$, $AgPF_6$, and $AgCF_3SO_3$). Different counteranions were employed for the preparation of the Ag(I) complexes to study their possible influence on the resulting supramolecular assembly.[60]

Molecular Structures with the $L^{H}PhS$ Ligand. Details of the data-collection parameters and other crystallographic information are given in Table 1, whereas experimental bond lengths and angles are provided in Table 2. $[Ag(L^{H}PhS)]_n(BF_4)_n$ exhibits a chain-like structure that is formed by the N_2 coordination on a metal center and by the bridging of the thioether group on a second metal. Two different types of silver atoms define the asymmetric unit. Both metal atoms are in a distorted T-shaped geometry (this is more pronounced for Ag(1) than for Ag(2)), which is distorted toward the tetrahedral geometry as a consequence of an Ag−C interaction that originates by one pyrazole ring for Ag(2) {d[Ag(2)−C(116)] = 2.773(6) Å} and by the peripheral phenyl ring for Ag(1) {d[(Ag(1)−C(24)] = 2.921(4) Å} (Figure 1). The absence of steric hindrance on the pyrazole rings allows for the approach of the Ag(2) atom over one of the pyrazole rings. The central phenyl ring of the ligand is oriented as previously found for bis(pyrazolyl) functionalized ligands.[39,40,61−67] This donor-set disposition favors the formation of metal−organic chains, and it is also the preferred conformation adopted by the ligands that exhibit a phenyl ring as a spacer between the bis(pyrazolyl) moiety and the thioether group (vide infra).

The molecular structure of $[Ag(L^{H}PhS)]_2(PF_6)_2$ is dinuclear, with the silver atom in a distorted T geometry (Figure 2). The donor atoms are represented by the N_2 chelate system of one ligand and by the S(13) and N(21) atoms of a symmetry-related ligand. Within the N_2 chelate group, the Ag−N(22) bond distance (2.238(3) Å) is significantly shorter than that of Ag−N(21) (2.428(3) Å). This fact is most likely a consequence of a weak π-interaction that the silver atom exchanges with the symmetry related N(21)′ atom (2.691(3) Å). The evidence that both nitrogen atoms interact with the metal is derived from the location of the silver atom above the ideal trigonal plane formed by the N(21), N(22), and S(13)′ donor atoms and directed toward the N(21)′ atom (symmetry code ′ = 1−x; 1−y; −z). As far as the ligand conformation is concerned, the central phenyl ring exhibits a conformation that is very close to that of $[Ag(L^{H}PhS)]_n(BF_4)_n$. The C(11) carbon atom of one pyrazole ring exchanges C−H···π interactions with the central phenyl ring of the symmetry-related ligand d[C(11)−C1t] = 3.622(4) Å, C1t: phenyl-ring centroid.

The dinuclear complex $[Cu(L^{H}PhS)(CH_3CN)]_2(BF_4)_2$ is obtained from the reaction between $[Cu(CH_3CN)_4]BF_4$ and

dx.doi.org/10.1021/ic201338w |Inorg. Chem. 2011, 50, 10786–10797

Table 2. Selected Bond Lengths (Å) and Angles (deg) for $[Ag(L^{H}PhS)]_n(BF_4)_n$, $[Cu(L^{H}PhS)(CH_3CN)]_2(BF_4)_2$, and $[Ag(L^{H}PhS)]_2(PF_6)_2$[a]

	$[Ag(L^{H}PhS)]_n(BF_4)_n$		
Ag(1)−N(21)	2.241(4)	Ag(2)−N(24)′	2.398(3)
Ag(1)−N(22)	2.384(4)	Ag(2)−N(25)′	2.316(4)
Ag(1)−S(16)	2.492(1)	Ag(2)−S(13)	2.529(1)
Ag(1)−C(24)	2.921(4)	Ag(2)−C(116)	2.773(6)
N(21)−Ag(1)−N(22)	87.7(1)	N(25)′−Ag(2)−N(24)′	83.0(1)
N(21)−Ag(1)−S(16)	171.1(1)	N(25)′−Ag(2)−S(13)	130.0(1)
N(22)−Ag(1)−S(16)	86.7(1)	N(24)′−Ag(2)−S(13)	117.36(9)
	$[Ag(L^{H}PhS)]_2(PF_6)_2$		
Ag−N(21)	2.428(3)	Ag−S(13)″	2.522(1)
Ag−N(22)	2.238(3)	Ag−N(21)″	2.691(3)
N(21)−Ag−N(22)	82.4(1)	N(22)−Ag−N(21)″	137.8(1)
N(21)−Ag−S(13)″	119.69(7)	N(22)−Ag−S(13)″	143.23(8)
N(21)−Ag−N(21)″	84.1(1)	N(21)″−Ag−S(13)″	75.05(9)
	$[Cu(L^{H}PhS)(CH_3CN)]_2(BF_4)_2$		
Cu−N(14)	1.944(3)	N(14)−Cu−N(22)	113.0(1)
Cu−N(21)	2.025(3)	N(21)−Cu−N(22)	93.9(1)
Cu−N(22)	2.028(3)	N(14)−Cu−S(13)‴	110.0(1)
Cu−S(13)‴	2.335(1)	N(21)−Cu−S(13)‴	105.4(1)
N(14)−Cu−N(21)	122.3(1)	N(22)−Cu−S(13)‴	111.0(1)

[a] Symmetry codes: ′ = 1/2+*x*; 1/2−*y*; *z*, ″ = 1−*x*; 1−*y*; −*z*, ‴ = 1−*x*; *y*; 1/2−*z*.

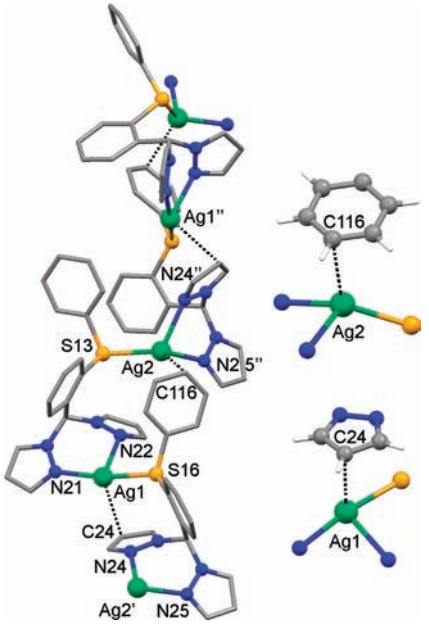

Figure 1. Molecular drawing of $[Ag(L^{H}PhS)]_n(BF_4)_n$. The BF_4^- anions and the hydrogen atoms are omitted for clarity.

$L^{H}PhS$. The metal shows a distorted tetrahedral geometry attained by the N_2 chelate system of one ligand, the thioether group of the second ligand, and an acetonitrile molecule (Figure 3). The phenyl ring acting as spacer is rotated approximately 60° with respect to the previous structures. The result of this arrangement is the S atom pointing toward the C−$H_{central}$, even though it is located at a noninteracting distance. Moreover,

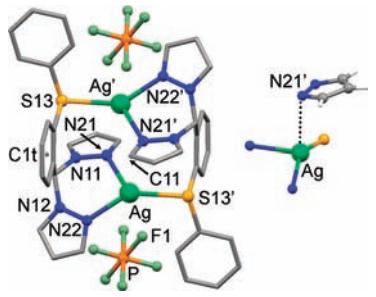

Figure 2. Molecular drawing of $[Ag(L^{H}PhS)]_2(PF_6)_2$. The hydrogen atoms are omitted for clarity. C1t, phenyl ring centroid, symmetry code ′ = 1−*x*; 1−*y*; −*z*.

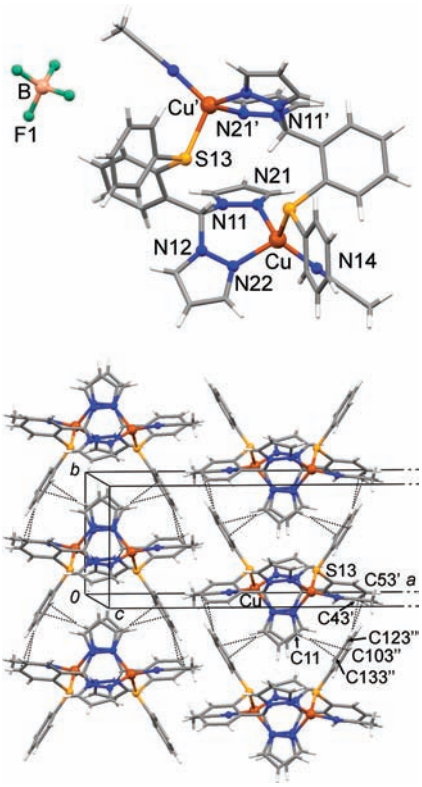

Figure 3. Molecular drawing of $[Cu(L^{H}PhS)(CH_3CN)]_2(BF_4)_2$, above, and a portion of the crystal packing, below. The BF_4^- anions are omitted for clarity. C−H···π interactions are represented by dashed bonds (below). Symmetry codes ′ = 1−*x*; *y*; 1/2−*z*, ″ = 1−*x*; *y*−1; 1/2−*z*.

the pyrazole rings also adopt a different conformation from that of $[Ag(L^{H}PhS)]_n(BF_4)_n$ and $[Ag(L^{H}PhS)]_2(PF_6)_2$ because their nitrogen lone pairs are oriented on the same side of the C−$H_{central}$. Obviously, this ligand conformation is unsuitable for the N_2S chelation because the C−$H_{central}$ is interposed between the N_2 and S donor atoms. From a pictorial point of view, the overall shape of the molecule resembles that of a cone delimited by alternate pyrazoles (those with N(12) and N(22)) and the peripheral phenyl rings. Two pyrazole rings on the opposite side of the cone face each other at a distance of 3.9 Å (measured from the centroids of the penta-atomic rings) with the minimum distance between symmetry-related N(21) and N(11) atoms (3.782(4) Å). The dinuclear units form pillars in which the

dx.doi.org/10.1021/ic201338w |*Inorg. Chem.* 2011, 50, 10786–10797

Table 3. Summary of X-ray Crystallographic Data for $[Ag(L^{H}CH_2S)]_n(BF_4)_n$, $[Ag(L^{iPr}CH_2S)]_n(PF_6)_n\cdot(CH_3)_2CO$, and $[Ag(L^{iPr}CH_2S)]_n(CF_3SO_3)_n\cdot 2CH_2Cl_2$

	$[Ag(L^{H}CH_2S)]_n(BF_4)_n$	$[Ag(L^{iPr}CH_2S)]_n(PF_6)_n\cdot(CH_3)_2CO$	$[Ag(L^{iPr}CH_2S)]_n(CF_3SO_3)_n\cdot 2CH_2Cl_2$
empirical formula	$C_{14}H_{14}AgBF_4N_4S$	$C_{55}H_{82}Ag_2F_{12}N_8OP_2S_2$	$C_{29}H_{42}AgCl_4F_3N_4O_3S_2$
formula weight	465.03	1441.09	865.46
color, habit	colorless, block	colorless, block	colorless, block
crystal size, mm	0.33 × 0.24 × 0.14	0.26 × 0.17 × 0.11	0.21 × 0.17 × 0.09
crystal system	monoclinic	monoclinic	monoclinic
space group	$P2_1/c$	Cc	$C2/c$
a, Å	8.901(1)	19.316(1)	23.477(2)
b, Å	17.268(2)	17.068(1)	12.839(1)
c, Å	11.510(1)	21.141(2)	26.057(2)
α, deg.	90	90	90
β, deg.	102.979(1)	102.624(2)	106.500(1)
γ, deg.	90	90	90
V, Å^3	1723.9(3)	6801.4(8)	7531(1)
Z	4	4	8
T, K	293(2)	293(2)	200(2)
ρ (calc), Mg/m^3	1.792	1.407	1.527
μ, mm^{-1}	1.335	0.758	0.980
θ range, deg.	2.17 to 30.51	1.61 to 26.86	1.63 to 26.75
no.of rflcn/unique	27964/5172	42584/14619	21169/7955
GOF	1.003	1.001	1.002
$R1$[a]	0.0380	0.0387	0.0493
$wR2$[a]	0.1094	0.0769	0.0612

[a] $R1 = \Sigma||F_o| - |F_c||/\Sigma|F_o|$, $wR2 = [\Sigma w(F_o^2 - F_c^2)^2/\Sigma w(F_o^2)^2]^{1/2}$, $w = 1/[\sigma^2(F_o^2) + (aP)^2 + bP]$, where $P = [\max(F_o^2,0) + 2F_c^2]/3$.

stacked pyrazole rings point inside the cone of another molecular unit. These pillars are held together by two types of C−H···π interactions that occur through (1) the C(11) pyrazole carbon atom and the peripheral phenyl ring, d[C(11)−C(103)″] = 3.629(5) Å, and d[C(11)−C(133)″] = 3.738(6) Å, and (2) through the central and peripheral phenyl rings, d[C(123)″−C(43)′] = 3.773(6) Å, and d[C(123)″−C(53)′] = 3.657(6) Å, symmetry codes ′ = 1−x; y; 1/2−z, ″ = 1−x; y−1; 1/2−z. Adjacent pillars are oriented in an antiparallel fashion, and they are aligned along the b crystallographic axis (Figure 3).

The Ag(I) and Cu(I) complexes with the L^{H}PhS ligand show a certain structural diversity when they exhibit dinuclear or polynuclear structures. Nevertheless, the invariant feature appears to be the inability of L^{H}PhS to chelate in the N_2S fashion. This ligand, in fact, behaves like an N_2 chelate with pyrazole rings and bridges to a different metal ion with the sulfur atom.

Molecular Structures with the $L^{R}CH_2S$ Ligand (R = H, Me, iPr). It is interesting to note that the complexes $[Ag(L^{H}CH_2S)]_n(BF_4)_n$, $[Ag(L^{Me}CH_2S)]_n(BF_4)_n$, $[Ag(L^{Me}CH_2S)]_n(CF_3SO_3)_n$, $[Ag(L^{Me}CH_2S)]_n(PF_6)_n$, $[Cu(L^{H}CH_2S)]_n(BF_4)_n$ and $[Cu(L^{Me}CH_2S)]_n(BF_4)_n$ exhibit very similar crystal structures (Table 3) despite the presence of different pyrazole ring substituents, metals or counter-anions. Also the supramolecular interactions responsible of the crystal packing are, from a qualitative point of view, identical. The molecular structures of these compounds will therefore be described together (Figures 4 and Supporting Information, Figures S1−S5). The metal adopts a distorted trigonal-planar geometry, with the N_2-chelating ligand attached to a metal center and bridging with the thioether sulfur atom on a symmetry-related metal ion. An inspection of the coordination bond distances indicates that, in the copper complexes $[Cu(L^{H}CH_2S)]_n(BF_4)_n$ and $[Cu(L^{Me}CH_2S)]_n(BF_4)_n$, the Cu−N separation varies in the relatively narrow range of 1.958(2)−2.053(2) Å, and the Cu−S bond distance is 2.17 Å for both compounds. On the other hand, the silver complexes $[Ag(L^{H}CH_2S)]_n(BF_4)_n$, $[Ag(L^{Me}CH_2S)]_n(BF_4)_n$, $[Ag(L^{Me}CH_2S)]_n(CF_3SO_3)_n$ and $[Ag(L^{Me}CH_2S)]_n(PF_6)_n$ present a greater variability with respect to the Ag−N bond distances, which are in the 2.203(2)−2.404(2) Å range. As for the copper complexes, the Ag−S distance is found in a more definite range of approximately 2.41 Å for all complexes (Table 4 and Supporting Information, Table S2).

The propensity of the ligand to bridge between two metal centers with the N_2 and S donor systems leads to the formation of zigzag chains that run parallel to the c crystallographic axis (Figure 4). To a different degree of strength, the chains interact with or are close to each other because of a partial stack of two symmetry-related pyrazole rings in the range of 3.612(4)−3.921(6) Å. This supramolecular interaction between the molecular chains forms a motif that may be described as perpendicular intersecting rectangles, which are occupied by the anions (BF_4^-, $CF_3SO_3^-$ or PF_6^-) (see Figure 4). Moreover, the view of the structure along the a crystallographic axis reveals how these molecular chains are organized in layers that are parallel to the bc crystallographic plane. We therefore infer that the counterion has little influence on the supramolecular aggregation of these complexes. The conformation of the central thioether arm influences the mode of interaction of the chains; in fact, the molecular structures of $[Cu(L^{H}CH_2S)]_n(BF_4)_n$, $[Ag(L^{H}CH_2S)]_n(BF_4)_n$ and $[Ag(L^{Me}CH_2S)]_n(PF_6)_n$ can be described by the conformation **A** depicted in Scheme 2, whereas the structures of $[Cu(L^{Me}CH_2S)]_n(BF_4)_n$, $[Ag(L^{Me}CH_2S)]_n(BF_4)_n$, and $[Ag(L^{Me}CH_2S)]_n(CF_3SO_3)_n$ are represented by the conformation **B**. The torsion

dx.doi.org/10.1021/ic201338w |Inorg. Chem. 2011, 50, 10786–10797

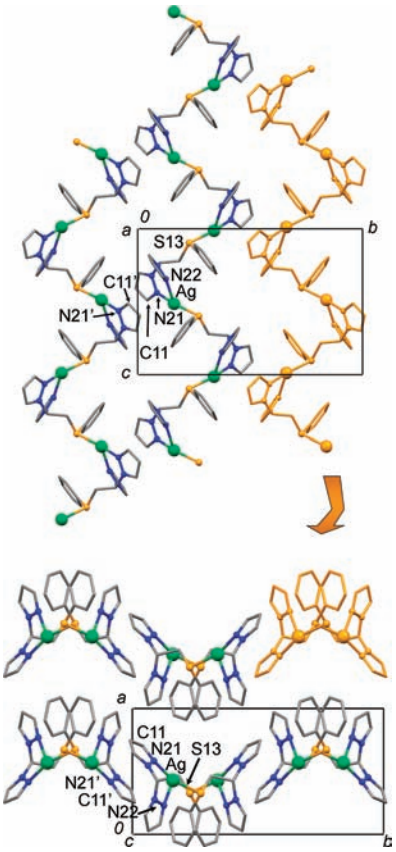

Figure 4. Crystal packing of $[Ag(L^{H}CH_2S)]_n(BF_4)_n$. View along the *a* axis (above), and along the *c* axis (below). The BF_4^- anions and the hydrogen atoms are omitted for clarity. Symmetry code ′ = 1−*x*; −*y*; 1−*z*.

angle (τ) involving the orientation of the thioether group with respect to the stacked pyrazole ring can be adopted as a stereochemical descriptor for discriminating between these two conformers. The τ values of the **A** and **B** conformations differ by approximately 120°. In all of these structures, the peripheral phenyl ring is always positioned above one of the pyrazole rings, thereby forming a partial π stack, with minimum distances in the range 3.205(6)−3.531(3) Å.

The complexes $[Ag(L^{iPr}CH_2S)]_n(PF_6)_n$ and $[Ag(L^{iPr}CH_2S)]_n(CF_3SO_3)_n$ form zigzag chains that are analogous to those of the previously described complexes (Figures 5 and 6). Nevertheless, the presence of the iPr groups as substituents on the pyrazole rings in place of the H or Me groups hinders the approach of the pyrazole rings of symmetry-related molecules. Hence, the chains do not form the intersecting rectangles observed in the previously described complexes. In $[Ag(L^{iPr}CH_2S)]_n(PF_6)_n$, the chains are organized in layers that are parallel to the *ab* crystallographic plane by interacting through the iPr and phenyl moieties, and the chains belonging to different planes are perpendicular to each other (see Figure 5). In contrast to the molecular structures reported thus far when using the $L^{R}CH_2S$ ligands, $[Ag(L^{iPr}CH_2S)]_n(CF_3SO_3)_n$ exhibits the silver atom in a distorted trigonal-pyramidal geometry as a consequence of the coordination of the $CF_3SO_3^-$ anion, *d*[Ag−O(24)] = 2.556(3) Å (Figure 6).

Molecular Structures with the $L^{R}PhS$ and $L^{R}CH_2S$ Ligands (R = H, Me) and Triphenylphosphine. To further investigate the coordinative behavior of the two classes of ligands, $L^{R}PhS$ and $L^{R}CH_2S$, we have employed triphenylphosphine (PPh_3) as an ancillary ligand for Cu(I) and Ag(I). Mixtures of equimolar amounts of $L^{R}PhS$ and $L^{R}CH_2S$ ligands, PPh_3, and $AgBF_4$ or $[Cu(CH_3CN)_4]BF_4$ result in the formation of easily recovered $[M(L)PPh_3]BF_4$ ternary complexes from the reaction mixture. The molecular structures of the Cu(I) complexes (Table 5) are reported in Figures 7 and 8 and in Supporting Information, Figures S6−S8. The presence of PPh_3 hinders the formation of coordination polymers so that all of the resulting complexes are mononuclear. The most striking difference between the complexes exhibiting the two different classes of ligands is the role played by the thioether group. In fact, in complexes $[Cu(L^{H}PhS)PPh_3]BF_4$ and $[Cu(L^{Me}PhS)PPh_3]BF_4$, the metal is in a distorted trigonal-planar geometry and is bound by the N_2 chelate ligand and PPh_3. The thioether group adopts the same

Table 4. Selected Bond Lengths (Å) and Angles (deg) for $[Ag(L^{H}CH_2S)]_n(BF_4)_n$, $[Ag(L^{iPr}CH_2S)]_n(PF_6)_n$, and $[Ag(L^{iPr}CH_2S)]_n(CF_3SO_3)_n$[a]

		$[Ag(L^{H}CH_2S)]_n(BF_4)_n$	
Ag−N(21)	2.203(2)	N(21)−Ag−N(22)	86.43(7)
Ag−N(22)	2.404(2)	N(21)−Ag−S(13)′	162.25(6)
Ag−S(13)′	2.4069(7)	N(22)−Ag−S(13)′	104.43(5)
		$[Ag(L^{iPr}CH_2S)]_n(PF_6)_n$	
Ag(1)−N(21)	2.272(3)	N(21)−Ag(1)−N(22)	81.8(1)
Ag(1)−N(22)	2.289(4)	N(21)−Ag(1)−S(16)″	136.19(8)
Ag(1)−S(16)″	2.419(1)	N(22)−Ag(1)−S(16)″	141.85(9)
Ag(2)−N(24)	2.268(3)	N(24)−Ag(2)−N(25)	84.6(1)
Ag(2)−N(25)	2.289(3)	N(24)−Ag(2)−S(13)	135.17(8)
Ag(2)−S(13)	2.429(1)	N(25)−Ag(2)−S(13)	140.24(9)
		$[Ag(L^{iPr}CH_2S)]_n(CF_3SO_3)_n$	
Ag−N(21)	2.288(3)	N(22)−Ag−N(21)	86.2(1)
Ag−N(22)	2.229(3)	N(22)−Ag−S(13)‴	130.25(9)
Ag−S(13)‴	2.433(1)	N(21)−Ag−S(13)‴	137.90(9)
Ag−O(24)	2.556(3)	N(22)−Ag−O(24)	98.1(1)
		N(21)−Ag−O(24)	105.8(1)
		O(24)−Ag−S(13)‴	90.71(7)

[a] Symmetry codes: ′ = *x*; 1/2−*y*; 1/2+*z*, ″ = *x*+1/2; *y*+1/2; *z*, ‴ = −*x*+1/2, *y*+1/2, −*z*+1/2.

Scheme 2. Depiction of the Conformations A and B, Which Describe the Intramolecular and Supramolecular Contacts of the Molecular Chains of Cu(I) and Ag(I) Complexes with the $L^{R}CH_2S$ Ligands

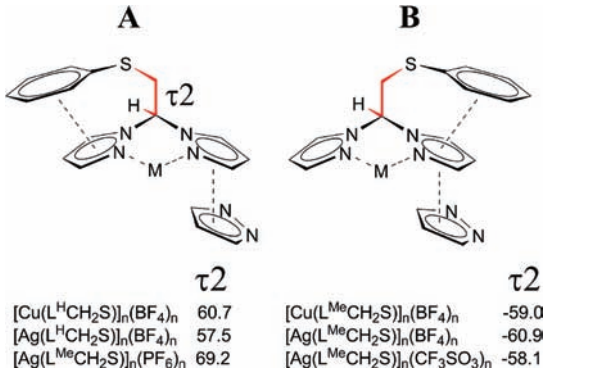

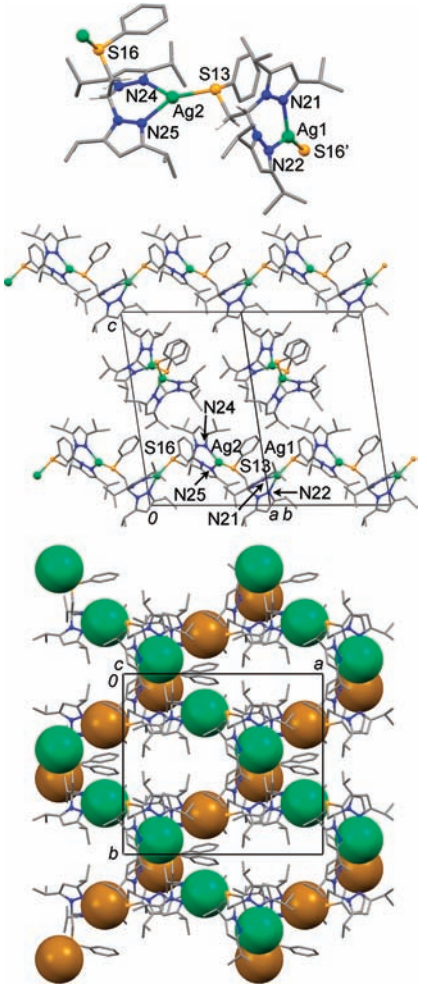

Figure 5. Molecular structure and crystal packing of $[Ag(L^{iPr}CH_2S)]_n(PF_6)_n$. The PF_6^- anions, the hydrogen atoms, and the solvent of crystallization are omitted for clarity. Green and brown spheres are the spacefill representations of the silver atoms, which depict the differently oriented molecular chains. Symmetry code $' = 1/2+x; 1/2+y; z$.

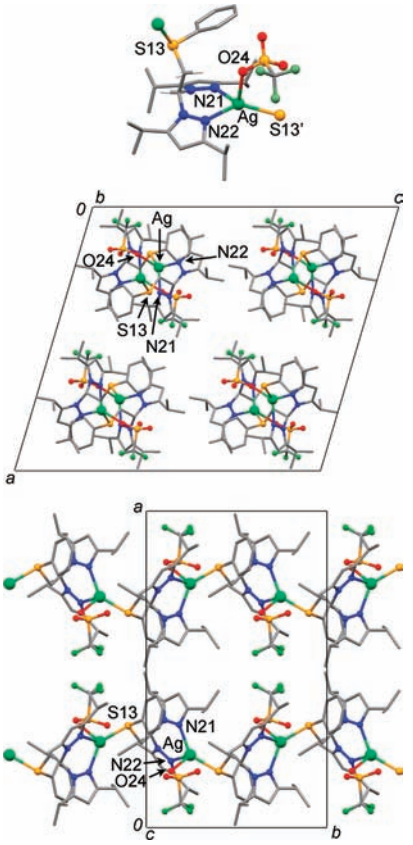

Figure 6. Molecular structure and crystal packing of $[Ag(L^{iPr}CH_2S)]_n(CF_3SO_3)_n$. The hydrogen atoms and the solvent of crystallization are omitted for clarity. Symmetry code $' = 1/2-x; 1/2+y; 1/2-z$.

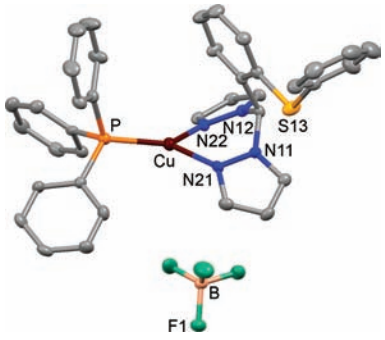

Figure 7. Molecular drawing of $[Cu(L^{H}PhS)PPh_3]BF_4$. Thermal ellipsoids are drawn at the 30% probability level. The hydrogen atoms are omitted for clarity.

conformation already described for the coordination polymers that were constructed with these ligands in the absence of PPh_3 (Scheme 3b). In contrast, $[Cu(L^{H}CH_2S)PPh_3]BF_4$, $[Cu(L^{Me}CH_2S)PPh_3]BF_4$, and $[Cu(L^{iPr}CH_2S)PPh_3]BF_4$ show the metal in a distorted tetrahedral geometry, and the ligands employ the N_2S donor set. In the present case, the thioether moiety is in a different conformation than that exhibited in the coordination polymers because the sulfur points to the same metal center of the N_2 donor system (Scheme 3d). In all the complexes, the Cu−N and Cu−P bond distances are in the 1.999(2)−2.065(3) Å and 2.161(6)−2.1863(7) Å ranges, respectively. In the $[Cu(L^{H}CH_2S)PPh_3]BF_4$, $[Cu(L^{Me}CH_2S)PPh_3]BF_4$, and $[Cu(L^{iPr}CH_2S)PPh_3]BF_4$ complexes, the Cu−S distance is in the narrow range of 2.4801(8)−2.4860(6) Å (Table 6 and Supporting Information, Table S5). Thus, the increase in the steric hindrance on the pyrazole rings when a hydrogen atom is substituted for an iPr group appears to neither affect the overall geometry of these complexes nor prevent the coordination of a relatively bulky ligand such as PPh_3.

The crystallization of the Cu(I) complexes reported here always affords colorless crystals of homogeneous shape. In contrast, during the crystallization of the Ag(I) complexes, a considerable number of crystals with hexagonal prismatic shapes are always present among the differently shaped prismatic crystals of the $[Ag(L)PPh_3]BF_4$ ternary complexes. The molecular structure derived from the X-ray diffraction analysis of the hexagonal crystals reveals that the compound is $[Ag(PPh_3)_4]BF_4$ (Supporting Information, Figure S12), which is isostructural with the previously reported complex $[Ag(PPh_3)_4]PF_6$.[68] Given the difficulties encountered during the recrystallization of the Ag(I) complexes, only the molecular structures of $[Ag(L^{H}PhS)PPh_3]BF_4$, $[Ag(L^{Me}CH_2S)PPh_3]BF_4$, and $[Ag(L^{iPr}CH_2S)PPh_3]BF_4$ could be obtained (Supporting Information, Figures S9−S11), and they

dx.doi.org/10.1021/ic201338w |Inorg. Chem. 2011, 50, 10786–10797

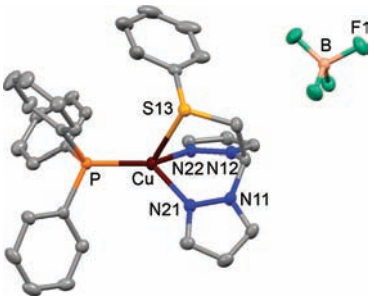

Figure 8. Molecular drawing of $[Cu(L^{H}CH_2S)PPh_3]BF_4 \cdot 1/2(C_3H_6O)$. Thermal ellipsoids are drawn at the 30% probability level. The hydrogen atoms are omitted for clarity.

Scheme 3. Description of the Coordinative Behavior of the Two Ligand Classes: Coordination Polymers (a, c) and Mononuclear Complexes Formed in Presence of Ancillary Ligands (b, d)

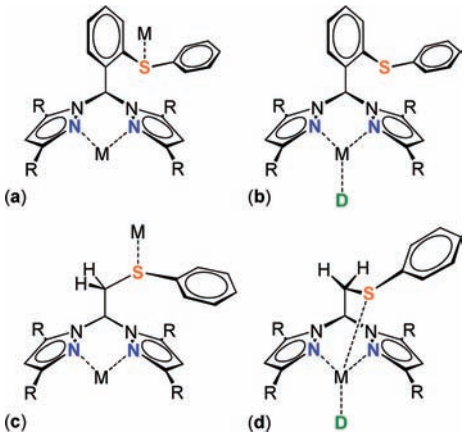

can be easily related to the corresponding Cu(I) complexes. In fact, in $[Ag(L^{H}PhS)PPh_3]BF_4$, the metal is in a trigonal-planar geometry achieved by the N_2 chelate ligand and PPh_3, with a thioether group that is not bound to the metal center. In contrast, the molecular structures of $[Ag(L^{Me}CH_2S)PPh_3]BF_4$, and $[Ag(L^{iPr}CH_2S)PPh_3]BF_4$ present the metal in a distorted tetrahedral geometry, and the $L^{Me}CH_2S$ and $L^{iPr}CH_2S$ ligands behave as N_2S tridentate. On average, the coordination bond distances of these silver complexes are more than 0.2 Å longer than those of the copper complexes, which is congruent with the larger size of the silver cation.

The molecular structures of these ternary complexes provide further evidence that the ligands with the methylene group as a spacer are coordinatively flexible. In contrast, the ligands with the phenyl ring as a spacer can be considered coordinatively rigid. Accordingly, their predominant conformation in the complexes presented thus far comprises the N_2 and S donor systems that are oriented in nearly opposite directions.

Conformational Studies. Conformational studies were performed to investigate the energetics relative to the mobilities of the pyrazole rings and thioether groups of the ligands. In a previous work, we investigated the coordination properties of a ligand system composed of a bis(pyrazolyl)methane system functionalized with a -SPhSPh bis-thioether group. To save computational resources, the peripheral -Ph-S-Ph moiety was replaced by a methyl group during the calculations.[40] In the present work, rigid

Table 5. Summary of X-ray Crystallographic Data for $[Cu(L^{H}PhS)PPh_3]BF_4 \cdot 1/2(C_3H_6O)$, $[Cu(L^{H}CH_2S)PPh_3]BF_4$

	$[Cu(L^{H}PhS)PPh_3]BF_4$	$[Cu(L^{H}CH_2S)PPh_3]BF_4 \cdot 1/2(C_3H_6O)$
empirical formula	$C_{37}H_{31}BCuF_4N_4PS$	$C_{33.5}H_{32}BCuF_4N_4O_{0.5}PS$
formula weight	745.04	712.01
color, habit	colorless, block	colorless, block
crystal size, mm	0.10 × 0.08 × 0.05	0.17 × 0.10 × 0.08
crystal system	monoclinic	triclinic
space group	$P2_1/n$	$P\bar{1}$
a, Å	13.953(4)	11.641(1)
b, Å	15.533(4)	11.854(1)
c, Å	16.860(5)	13.121(1)
α, deg.	90	79.685(1)
β, deg.	106.95(1)	77.861(1)
γ, deg.	90	70.546(1)
V, Å^3	3495(2)	1657.3(2)
Z	4	2
T, K	190(2)	200(2)
ρ (calc), Mg/m^3	1.416	1.427
μ, mm^{-1}	0.785	0.825
θ range, deg.	1.67 to 26.00	1.60 to 23.26
no.of rflcn/unique	36407/6857	14162/4761
GOF	0.775	1.006
$R1^a$	0.0490	0.0242
$wR2^a$	0.0509	0.0627

$^a R1 = \Sigma||F_o| - |F_c||/\Sigma|F_o|$, $wR2 = [\Sigma w(F_o^2 - F_c^2)^2/\Sigma w(F_o^2)^2]^{1/2}$, $w = 1/[\sigma^2(F_o^2) + (aP)^2 + bP]$, where $P = [\max(F_o^2,0) + 2F_c^2]/3$.

Table 6. Selected Bond Lengths (Å) and Angles (deg) for $[Cu(L^{H}PhS)PPh_3]BF_4$, $[Cu(L^{H}CH_2S)PPh_3]BF_4 \cdot 1/2(C_3H_6O)$

	$[Cu(L^{H}PhS)PPh_3]BF_4$		
Cu−N(21)	2.000(3)	N(21)−Cu−N(22)	92.0(1)
Cu−N(22)	2.010(3)	N(21)−Cu−P	136.95(9)
Cu−P	2.175(1)	N(22)−Cu−P	131.08(9)
	$[Cu(L^{H}CH_2S)PPh_3]BF_4 \cdot 1/2(C_3H_6O)$		
Cu−N(21)	2.030(2)	N(21)−Cu−N(22)	90.55(6)
Cu−N(22)	2.037(2)	N(21)−Cu−P	130.80(5)
Cu−S(13)	2.4860(6)	N(22)−Cu−P	126.13(4)
Cu−P	2.1656(5)	N(21)−Cu−S(13)	90.63(5)
		N(22)−Cu−S(13)	88.81(5)
		P−Cu−S(13)	118.15(2)

PES scans are performed using the two real systems $L^{H}PhS$ and $L^{H}CH_2S$ as benchmarks for the investigation of the flexibility of the two ligand classes. The calculations are performed by varying three torsion angles; $\tau 1$ rotates one of the pyrazole rings, $\tau 2$ rotates the spacer between the thioether and bis(pyrazolyl)-methane moieties (Ph or CH_2), and $\tau 3$ rotates the peripheral phenyl ring. Because the calculations are performed without optimization at every step (rigid PES scan), there are unrealistic conformations in which the phenyl, pyrazole or thioether groups collide with one another. These conformations are characterized by very high energy and will not be discussed further.

dx.doi.org/10.1021/ic201338w |Inorg. Chem. 2011, 50, 10786–10797

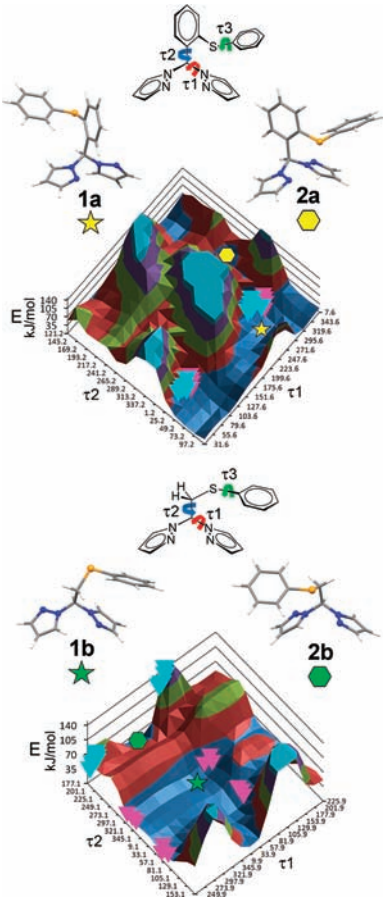

Figure 9. Rigid PES scan of the $L^{H}PhS$ and $L^{H}CH_2S$ ligands. For both ligand classes, the conformations corresponding to the potential N_2 and N_2S coordination behavior are indicated by the ★ and ⬢ symbols, respectively. The conformations adopted by the ligands in the polynuclear $[M(L)]_n^{n+}$ and mononuclear $[M(L)PPh_3]BF_4$ complexes are indicated with purple and magenta triangles, respectively.

The conformation of $L^{H}PhS$ that exhibits the minimum energy is **1a** reported in Figure 9. This conformation is characterized by the pyrazole ring that orients the nitrogen lone pair on approximately the same side of the molecule ($\tau1$ = 295.6°) and by the thioether group that points toward the methine proton ($\tau2$ = 49.2°). Because of the arrangement of the phenyl spacer group, the peripheral phenyl ring does not interact with any other molecular fragment ($\tau3$ = 342.1°). This lack of interaction has consequences for the energies involved in the free rotation of this group because only 14 kJ/mol are required when $\tau1$ = 295.6° and $\tau2$ = 49.2°. The 360° rotation of the pyrazole ring ($\tau1$) requires 24 kJ/mol when $\tau2$ = 49.2° and $\tau3$ = 342.1°. In comparison, the rotation of the thioether group requires at least 90 kJ/mol (with $\tau1$ = 295.6° and $\tau2$ = 49.2°). Furthermore, an inspection of all PES scans reported in the Supporting Information reveals how the pyrazole rotation is an energetically relatively inexpensive process, whereas the rotation of the phenyl ring acting as a spacer usually implies high energy barriers. In particular, the regions of the PES scans characterized by minor energy are those that are associated with the conformation in which the thioether points toward the central methine proton ($\tau2$ range of = 25.2−73.2°). Structure **2a** corresponds to the ligand conformation that would allow the N_2S coordination of this ligand class, and its energy is at least 30 kJ/mol greater than that of **1a**. This is a modest value in absolute terms, but an inspection of the PES scans indicates that this conformation is surrounded by regions of higher energy. Therefore, it is possible that the conformational modification derived from the N_2S chelation would be associated with a destabilization that rules out this mode of binding for the $L^{H}PhS$ ligand.

The $L^{H}CH_2S$ ligand should be characterized by a greater flexibility when compared to the $L^{R}PhS$ ligand class. This is evident when examining the PES scan of $L^{H}CH_2S$, because the regions of low energy are more extensive than those of the $L^{H}PhS$ PES scan. The conformation of $L^{H}CH_2S$ that exhibits the minimum energy is **1b** reported in Figure 9. This conformation is characterized by (1) pyrazole rings oriented in an antiparallel fashion ($\tau1$ = 57.9°), (2) the methylene bridge and the central methine proton in a staggered conformation with the thioether that points toward the methine proton ($\tau2$ = 321.1°), and (3) the peripheral phenyl ring nearly staked over one of the pyrazole rings ($\tau3$ = 288.1°). On the basis of the analysis of the PES scan, the rotation of the phenyl ring is the least energetically demanding (∼20 kJ/mol), and the most stable conformation presumably attains a slight stabilization by the partial π-stack of the pyrazole and phenyl rings. Also, the rotation of the pyrazole ring requires a limited expenditure of energy: ∼33 kJ/mol for a 360° rotation of $\tau1$ when $\tau2$ = 321.1° and $\tau3$ = 288.1°. The rotation of the thioether group requires slightly more energy, but it is still energetically a relatively inexpensive process: ∼52 kJ/mol for a 360° rotation of $\tau2$ when $\tau1$ = 57.9° and $\tau3$ = 288.1°. Furthermore, by a close inspection of the various energy profiles of $L^{R}CH_2S$ provided in Figure 9 and the Supporting Information, it is evident that there are a number of conformations that are very close in energy; they can be grouped into two main reference structures: one corresponds to the minimum of the PES scan, as previously described (**1b** in Figure 9), whereas the other is still characterized by a staggered conformation of the methylene and methine protons but with the sulfur atoms pointing to the opposite side of the central methine proton (**2b** in Figure 9). This latter conformation, apart from the rotation of one pyrazole ring, is the one adopted by the ligand in the ternary complexes in the presence of PPh_3.

Figure 9 also includes the experimental geometric parameters $\tau1$ and $\tau2$ that were derived by the X-ray structural analyses of the complexes obtained with the two ligand systems. Because the PES was derived for the free ligands, the energies associated with the coordination to the metal ion are expected to result in a considerable modification of the two surfaces. Nevertheless, it is helpful to visualize where the $\tau1$-$\tau2$ geometric parameters of the complexes are positioned on the two free-ligand PESs. For both systems, it is evident that the $\tau1$ experimental values are localized in two regions (∼60 and ∼300°), and these are associated with the pyrazole rings oriented in a favorable position to chelate the metal ions.[69] As far as the $\tau2$ value is concerned, for $L^{R}PhS$ it varies in a narrow range at approximately 0°, which is associated with a geometry very close to that of **1a**. For $L^{R}CH_2S$, however, there are three regions in which $\tau2$ varies, but they can be reduced to two regions because $\tau2$ values of approximately 60 and 300° arise by the centrosymetrically related molecules in the crystal lattice (ligand N_2 chelates and bridges with S). In particular, they refer to enantiomerically related fragments in which the peripheral phenyl ring is oriented over one or the other pyrazole rings. The other region where the experimental $\tau2$ values are clustered (∼180°) is related to the PPh_3 complexes in which the ligands

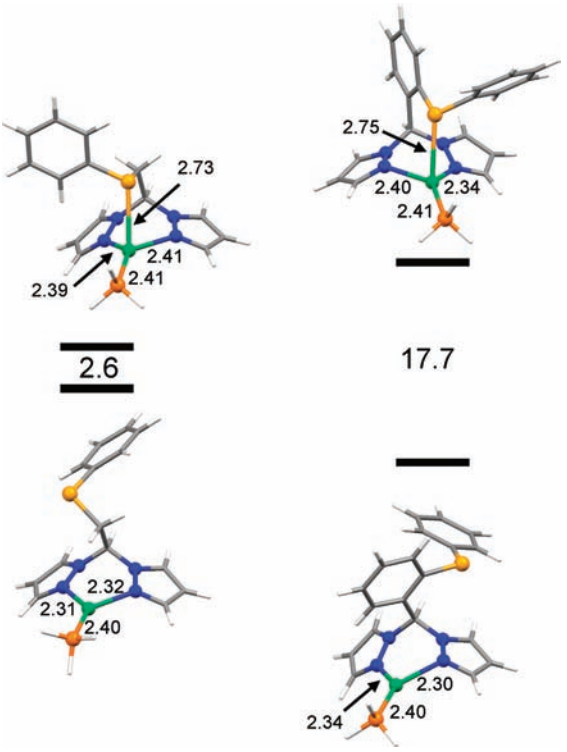

Figure 10. Energy differences (kJ/mol) between the coordination isomers of the two model complexes, $[Ag(L^{H}PhS)PH_3]^+$ and $[Ag(L^{H}CH_2S)PH_3]^+$ (B3LYP/6-31+G(d)-SDD). Selected coordination bond distances (Å) are reported.

behave as a N_2S donor. The preferred conformations of the free ligand (**1b** and **2b**) present the pyrazole rings oriented in an antiparallel fashion, whereas the nitrogen lone pairs converge to the metal center in the complexes. As previously noted, this conformation determines the localization of the experimental geometry on PES regions of relatively high energy.

Bearing this consideration in mind, it is nevertheless evident that the $L^{R}PhS$ ligand class is conformationally more rigid and preorganized than the $L^{R}CH_2S$ class. In fact, the general and therefore expected behavior of the $L^{R}PhS$ ligands is the N_2 chelation on a metal and possibly the bridging interaction of the thioether group on a second metal. The presence of the phenyl group as a spacer precludes the N_2S chelation mode for this ligand class. In contrast, the $L^{R}CH_2S$ class usually N_2 chelates and bridges with the thioether group on a second metal, but it can also act as a N_2S donor on the same metal ion. The energy expenditure to drive the thioether and the bis(pyrazolyl)methane systems to chelate the same metal ion is compensated by the metal−sulfur interaction energy, which is evidently not sufficient for the $L^{R}PhS$ system.

This compensation is further evidenced by inspecting the energy profiles of the conformational isomers of the two model complexes, $[Ag(L^{H}PhS)PH_3]^+$ and $[Ag(L^{H}CH_2S)PH_3]^+$ (Figure 10). For $[Ag(L^{R}CH_2S)PH_3]^+$, the energy difference between the two isomers is only 2.6 kJ/mol, which confirms that there is not a significant energy gain derived by the coordination of the thioether group when a metal ion is present. In contrast, for $[Ag(L^{H}PhS)PH_3]^+$, the isomer with the N_2S chelate ligand lies 17.7 kJ/mol above that of the isomer with the N_2 bidentate ligand. An inspection of the optimized molecular structure of this complex indicates that the sulfur coordination implies a certain ligand strain. In particular, the sulfur coordination requires a destabilizing approach between the $CH_{central}$ and the CH_{ortho} hydrogen atoms.

CONCLUSIONS

Rigid ligand systems are those usually characterized by one stable conformation or configuration that exhibits a definite orientation of the donor atom's lone pairs that are involved in metal binding. If the stereoelectronic properties of the metal match this preferred orientation, the result is usually the formation of a stable metal complex. Nevertheless, interesting situations arise when the lone-pair directionality and metal requirements are mismatched. In particular, when an unusual geometry is forced on a metal center, the result is an increase in the energetic state of the system (entatic state).[70,71] This concept was originally developed for metal sites in biological systems, such as metallo-proteins, but it has a general valence and has been recently exploited for the construction of metal−organic frameworks to enhance gas-sorption properties[72] or to force a metal ion to adopt unusual spin states.[17] In contrast, flexible ligand systems are characterized by a number of conformations that are similar in energy and may be adopted by the ligand in response to the metal presence or external stimuli.[16] Flexible systems have also found applications in the realization of dynamic coordination polymers that are subject to structural modification when interacting with guest molecules.[73]

In the present work, the coordination properties and conformational rigidity/flexibility of two ligand classes were investigated. These ligands are relevant for the construction of coordination polymers and they are characterized by the N_2S mixed donor set derived from a bis(pyrazolyl)methane system and a thioether function. However, the spacer between these two donor systems exhibits a considerable influence on the coordination properties of the ligands. The phenyl group in $L^{R}PhS$ renders these systems more rigid from a conformational point of view, and in all of the reported molecular structures the phenyl spacer is always approximately parallel to the $C_{central}$-N_{pz} bond. The geometric consequences are such that the bis(pyrazolyl)-methane moiety is oriented in approximately the opposite direction of the thioether group, and polynuclear complexes are usually formed. In contrast, the $L^{R}CH_2S$ ligand class is inherently more flexible, because two thioether arrangements are energetically accessible that are associated with the following binding modes: the N_2S chelation, and the and N_2 chelation on a metal and the bridging on a second metal with the sulfur atom. Nevertheless, as attested by the molecular structures of the $[M(L^{R}CH_2S)]^+$ binary complexes, the N_2 chelation and S-bridging on a second metal is the preferred conformation adopted by the $L^{R}CH_2S$ ligand class. In fact, molecular chains are invariably formed for these type of complexes, and they present very similar crystal packing when R = H or Me. When the steric hindrance of the pyrazole rings is increased (R = iPr), the supramolecular interaction that is observed between the chains of the less-encumbered ligands are no longer displayed, even though the chains are still formed.

The experimental evidence pertaining to the different binding modes of the two ligand classes are confirmed by computational studies on two representative ligands: $L^{H}CH_2S$ and $L^{H}PhS$. According to these calculations, the free rotation of the thioether group in $L^{H}CH_2S$ and $L^{H}PhS$ requires ∼50 kJ/mol and ∼90 kJ/mol, respectively, confirming the more flexible nature of $L^{H}CH_2S$ when compared to $L^{H}PhS$.

The different coordinative behavior between the two ligand classes is more clearly evidenced in the ternary complexes $[M(L)PPh_3]^+$ (M = Cu(I) or Ag(I); L = L^RCH_2S or L^RPhS), where the presence of PPh_3 hinders the formation of polymeric structures and favors the formation of mononuclear complexes. In these types of complexes, the L^RCH_2S ligands act as a N_2S chelate that yields a distorted tetrahedral metal geometry, whereas the L^RPhS ligands employ only the bis(pyrazolyl)methane system for the metal coordination and the thioether group is oriented as in the binary complexes but does not contribute to the metal binding.

In summary, the most stable conformations for both ligand systems are those associated with the N_2 and S donor systems pointing in nearly opposite directions, which makes these ligands suitable for the formation of polymeric structures.

■ ASSOCIATED CONTENT

Supporting Information. Synthesis of Ag(I) and Cu(I) complexes. Crystallographic information files (CIF). Cartesian coordinates of the optimized structures (B3LYP/SDD-6-31+G-(d)) of the two conformational isomers of the model complexes $[Ag(L^HCH_2S)PH_3]^+$ and $[Ag(L^HPhS)PH_3]^+$. This material is available free of charge via the Internet at http://pubs.acs.org.

■ AUTHOR INFORMATION

Corresponding Author
*E-mail: marchio@unipr.it.

■ ACKNOWLEDGMENT

This work was supported by the Università degli Studi di Parma (Parma, Italy).

■ REFERENCES

(1) Khlobystov, A. N.; Blake, A. J.; Champness, N. R.; Lemenovskii, D. A.; Majouga, A. G.; Zyk, N. V.; Schroder, M. *Coord. Chem. Rev.* **2001**, *222*, 155–192.
(2) Robin, A. Y.; Fromm, K. M. *Coord. Chem. Rev.* **2006**, *250*, 2127–2157.
(3) Janiak, C.; Vieth, J. K. *New J. Chem.* **2010**, *34*, 2366–2388.
(4) Leong, W. L.; Vittal, J. J. *Chem. Rev.* **2011**, *111*, 688–764.
(5) Uemura, T.; Yanai, N.; Kitagawa, S. *Chem. Soc. Rev.* **2009**, *38*, 1228–1236.
(6) Rowsell, J. L. C.; Spencer, E. C.; Eckert, J.; Howard, J. A. K.; Yaghi, O. M. *Science* **2005**, *309*, 1350–1354.
(7) Britt, D.; Tranchemontagne, D.; Yaghi, O. M. *Proc. Natl. Acad. Sci. U.S.A.* **2008**, *105*, 11623–11627.
(8) Wu, H.; Zhou, W.; Yildirim, T. *J. Am. Chem. Soc.* **2009**, *131*, 4995–5000.
(9) Kitagawa, S. *Nature* **2006**, *441*, 584–585.
(10) Kitagawa, S.; Kitaura, R.; Noro, S. *Angew. Chem., Int. Ed.* **2004**, *43*, 2334–2375.
(11) Seward, C.; Jia, W. L.; Wang, R. Y.; Enright, G. D.; Wang, S. N. *Angew. Chem., Int. Ed.* **2004**, *43*, 2933–2936.
(12) Xie, Z. G.; Ma, L. Q.; deKrafft, K. E.; Jin, A.; Lin, W. B. *J. Am. Chem. Soc.* **2010**, *132*, 922–923.
(13) Yuan, M.; Zhao, F.; Zhang, W.; Wang, Z. M.; Gao, S. *Inorg. Chem.* **2007**, *46*, 11235–11242.
(14) Li, B.; Gu, W.; Zhang, L. Z.; Qu, J.; Ma, Z. P.; Liu, X.; Liao, D. Z. *Inorg. Chem.* **2006**, *45*, 10425–10427.
(15) Imaz, I.; Rubio-Martinez, M.; Garcia-Fernandez, L.; Garcia, F.; Ruiz-Molina, D.; Hernando, J.; Puntes, V.; Maspoch, D. *Chem. Commun.* **2010**, *46*, 4737–4739.
(16) Comba, P.; Schiek, W. *Coord. Chem. Rev.* **2003**, *238*, 21–29.
(17) Comba, P.; Kerscher, M.; Lawrance, G. A.; Martin, B.; Wadepohl, H.; Wunderlich, S. *Angew. Chem., Int. Ed.* **2008**, *47*, 4740–4743.
(18) Chakraborty, B.; Halder, P.; Paine, T. K. *Dalton Trans.* **2011**, *40*, 3647–3654.
(19) Little, M. A.; Halcrow, M. A.; Harding, L. P.; Hardie, M. J. *Inorg. Chem.* **2010**, *49*, 9486–9496.
(20) Libri, S.; Mahler, M.; Espallargas, G. M.; Singh, D. C. N. G.; Soleimannejad, J.; Adams, H.; Burgard, M. D.; Rath, N. P.; Brunelli, M.; Brammer, L. *Angew. Chem., Int. Ed.* **2008**, *47*, 1693–1697.
(21) Steel, P. J.; Fitchett, C. M. *Coord. Chem. Rev.* **2008**, *252*, 990–1006.
(22) Uemura, K.; Kumamoto, Y.; Kitagawa, S. *Chem.—Eur. J.* **2008**, *14*, 9565–9576.
(23) Niu, C. Y.; Wu, B. L.; Zheng, X. F.; Zhang, H. Y.; Li, Z. J.; Hou, H. W. *Dalton Trans.* **2007**, 5710–5713.
(24) Zhang, J. P.; Horike, S.; Kitagawa, S. *Angew. Chem., Int. Ed.* **2007**, *46*, 889–892.
(25) Jouaiti, A.; Hosseini, M. W.; Kyritsakas, N.; Grosshans, P.; Planeix, J. M. *Chem. Commun.* **2006**, 3078–3080.
(26) Nagarathinam, M.; Vittal, J. J. *Angew. Chem., Int. Ed.* **2006**, *45*, 4337–4341.
(27) (a) Schmidbaur, H.; Schier, A. *Chem. Soc. Rev.* **2008**, *37*, 1931–1951. (b) Pyykko, P. *Chem. Rev.* **1997**, *97*, 597–636. Though the metallophilic interaction among the coinage metals is strongest for gold, the occurrence of this interaction is well represented in the literature among silver complexes, see:(a) Yuan, G.; Zhu, C.; Liu, Y.; Xuan, W.; Cui, Y. *J. Am. Chem. Soc.* **2009**, *131*, 10452–10460. (b) Samantaray, M. K.; Pang, K.; Shaikh, M .M.; Ghosh, P. *Inorg. Chem.* **2008**, *47*, 4153–4165. (c) Carranza, M. P.; Manzano, B. R.; Jalon, F. A.; Rodrýguez, A. M.; Santos, L.; Moreno, M. *Inorg. Chem.* **2010**, *49*, 3828–3835. (d) Serpe, A.; Artizzu, F.; Marchiò, L.; Mercuri, M. L.; Pilia, L.; Deplano, P. *Cryst. Growth Des.* **2011**, *11*, 1278–1286.
(28) Dias, H. V. R.; Singh, S.; Campana, C. F. *Inorg. Chem.* **2008**, *47*, 3943–3945.
(29) Tyrra, W.; Aboulkacem, S.; Pantenburg, I. *J. Organomet. Chem.* **2006**, *691*, 514–522.
(30) Zhao, L.; Mak, T. C. W. *J. Am. Chem. Soc.* **2005**, *127*, 14966–14967.
(31) Yang, L. Y.; Shan, W. F.; Chen, Q. Q.; Wang, Z. P.; Ma, J. S. *Eur. J. Inorg. Chem.* **2004**, 1474–1477.
(32) Munakata, M.; Ning, G. L.; Suenaga, Y.; Kuroda-Sowa, T.; Maekawa, M.; Ohta, T. *Angew. Chem., Int. Ed.* **2000**, *39*, 4555–4557.
(33) Reger, D. L.; Foley, E. A.; Semenluc, R. F.; Smith, M. D. *Inorg. Chem.* **2007**, *46*, 11345–11355.
(34) Reger, D. L.; Foley, E. A.; Smith, M. D. *Inorg. Chem.* **2010**, *49*, 234–242.
(35) Reger, D. L.; Watson, R. P.; Smith, M. D. *Inorg. Chem.* **2006**, *45*, 10077–10087.
(36) Reger, D. L.; Watson, R. P.; Gardinier, J. R.; Smith, M. D. *Inorg. Chem.* **2004**, *43*, 6609–6619.
(37) Chandrasekhar, V.; Thilagar, P.; Senapati, T. *Eur. J. Inorg. Chem.* **2007**, 1004–1009.
(38) Santillan, G. A.; Carrano, C. J. *Inorg. Chem.* **2008**, *47*, 930–939.
(39) Santillan, G. A.; Carrano, C. J. *Cryst. Growth Des.* **2009**, *9*, 1590–1598.
(40) Gennari, M.; Bassanetti, I.; Marchiò, L. *Polyhedron* **2010**, *29*, 361–371.
(41) The, K. I.; Peterson, L. K. *Can. J. Chem.* **1973**, *51*, 422–426.
(42) The, K. I.; Peterson, L. K.; Kiehlmann, E. *Can. J. Chem.* **1973**, *51*, 2448–2451.
(43) Peterson, L. K.; Kiehlmann, E.; Sanger, A. R.; The, K. I. *Can. J. Chem.* **1974**, *52*, 2367–2374.
(44) Tardito, S.; Bassanetti, I.; Bignardi, C.; Elviri, L.; Tegoni, M.; Mucchino, C.; Bussolati, O.; Franchi-Gazzola, R.; Marchiò, L. *J. Am. Chem. Soc.* **2011**, *133*, 6235–6242.
(45) *SMART* (control) and *SAINT* (integration) software for CCD systems; Bruker AXS: Madison, WI, 1994.

(46) *SADABS, Area-Detector Absorption Correction*; Siemens Industrial Automation Inc.: Madison, WI, 1996.
(47) Altomare, A.; Burla, M. C.; Camalli, M.; Cascarano, G. L.; Giacovazzo, C.; Guagliardi, A.; Moliterni, A. G. G.; Polidori, G.; Spagna, R. *J. Appl. Crystallogr.* **1999**, *32*, 115–119.
(48) Burla, M. C.; Caliandro, R.; Camalli, M.; Carrozzini, B.; Cascarano, G. L.; De Caro, L.; Giacovazzo, C.; Polidori, G.; Spagna, R. *J. Appl. Crystallogr.* **2005**, *38*, 381–388.
(49) Sheldrick, G. M. *SHELX97, Programs for Crystal Structure Analysis*, release 97-2; University of Göttingen: Göttingen, Germany, 1997.
(50) Farrugia, L. J. *J. Appl. Crystallogr.* **1999**, *32*, 837–838.
(51) Macrae, C. F.; Edgington, P. R.; McCabe, P.; Pidcock, E.; Shields, G. P.; Taylor, R.; Towler, M.; van de Streek, J. *J. Appl. Crystallogr.* **2006**, *39*, 453–457.
(52) Becke, A. D. *Phys. Rev. A* **1988**, *38*, 3098–3100.
(53) Becke, A. D. *J. Chem. Phys.* **1993**, *98*, 5648–5652.
(54) Ditchfield, R.; Hehre, W. J.; Pople, J. A. *J. Chem. Phys.* **1971**, *54*, 724–728.
(55) Rassolov, V. A.; Ratner, M. A.; Pople, J. A.; Redfern, P. C.; Curtiss, L. A. *J. Comput. Chem.* **2001**, *22*, 976–984.
(56) Fuentealba, P.; Preuss, H.; Stoll, H.; v. Szentpaly, L. *Chem. Phys. Lett.* **1982**, *89*, 418–422.
(57) Cao, X. Y.; Dolg, M. *J. Mol. Struct.* **2002**, *581*, 139–147.
(58) Schwerdtfeger, P.; Dolg, M.; Schwarz, W. H. E.; Bowmaker, G. A.; Boyd, P. D. W. *J. Chem. Phys.* **1989**, *91*, 1762–1774.
(59) Frisch, M. J.; Trucks, G. W.; Schlegel, H. B.; Scuseria, G. E.; Robb, M. A.; Cheeseman, J. R.; Montgomery, Jr., J. A.; Vreven, T.; Kudin, K. N.; Burant, J. C.; Millam, J. M.; Iyengar, S. S.; Tomasi, J.; Barone, V.; Mennucci, B.; Cossi, M.; Scalmani, G.; Rega, N.; Petersson, G. A.; Nakatsuji, H.; Hada, M.; Ehara, M.; Toyota, K.; Fukuda, R.; Hasegawa, J.; Ishida, M.; Nakajima, T.; Honda, Y.; Kitao, O.; Nakai, H.; Klene, M.; Li, X.; Knox, J. E.; Hratchian, H. P.; Cross, J. B.; Bakken, V.; Adamo, C.; Jaramillo, J.; Gomperts, R.; Stratmann, R. E.; Yazyev, O.; Austin, A. J.; Cammi, R.; Pomelli, C.; Ochterski, J. W.; Ayala, P. Y.; Morokuma, K.; Voth, G. A.; Salvador, P.; Dannenberg, J. J.; Zakrzewski, V. G.; Dapprich, S.; Daniels, A. D.; Strain, M. C.; Farkas, O.; Malick, D. K.; Rabuck, A. D.; Raghavachari, K.; Foresman, J. B.; Ortiz, J. V.; Cui, Q.; Baboul, A. G.; Clifford, S.; Cioslowski, J.; Stefanov, B. B.; Liu, G.; Liashenko, A.; Piskorz, P.; Komaromi, I.; Martin, R. L.; Fox, D. J.; Keith, T.; Al-Laham, M. A.; Peng, C. Y.; Nanayakkara, A.; Challacombe, M.; Gill, P. M. W.; Johnson, B.; Chen, W.; Wong, M. W.; Gonzalez, C.; and Pople, J. A. *Gaussian 03*, Revision C.02; Gaussian, Inc.: Wallingford, CT, 2004.
(60) Halper, S. R.; Do, L.; Stork, J. R.; Cohen, S. M. *J. Am. Chem. Soc.* **2006**, *128*, 15255–15268.
(61) Santillan, G. A.; Carrano, C. J. *Inorg. Chem.* **2007**, *46*, 1751–1759.
(62) Milione, S.; Capacchione, C.; Cuomo, C.; Strianese, M.; Bertolasi, V.; Grassi, A. *Inorg. Chem.* **2009**, *48*, 9510–9518.
(63) Elflein, J.; Platzmann, F.; Burzlaff, N. *Eur. J. Inorg. Chem.* **2007**, 5173–5176.
(64) Carrion, M. C.; Diaz, A.; Guerrero, A.; Jalon, F. A.; Manzano, B. R.; Rodriguez, A.; Paul, R. L.; Jeffery, J. C. *J. Organomet. Chem.* **2002**, *650*, 210–222.
(65) Carrion, M. C.; Jalon, F. A.; Manzano, B. R.; Rodriguez, A. M.; Sepulveda, F.; Maestro, M. *Eur. J. Inorg. Chem.* **2007**, 3961–3973.
(66) Carrion, M. C.; Sepulveda, F.; Jalon, F. A.; Manzano, B. R.; Rodriguez, A. M. *Organometallics* **2009**, *28*, 3822–3833.
(67) Santillan, G. A.; Carrano, C. J. *Dalton Trans.* **2009**, 6599–6605.
(68) Cotton, F. A.; Luck, R. L. *Acta Crystallogr., Sect. C: Cryst. Struct. Commun.* **1989**, *45*, 1222–1223.
(69) The two regions arise by the presence of centrosymetrically related molecules in the crystal lattice.
(70) Vallee, B. L.; Williams, R. J. P. *Proc. Natl. Acad Sci. U.S.A.* **1968**, *59*, 498–505.
(71) Williams, R. J. P. *Eur. J. Biochem.* **1995**, *234*, 363–381.
(72) Ma, S. Q.; Zhou, H. C. *J. Am. Chem. Soc.* **2006**, *128*, 11734–11735.
(73) Kitagawa, S.; Matsuda, R. *Coord. Chem. Rev.* **2007**, *251*, 2490–2509.